Diagn Interv Radiol 2025; DOI: 10.4274/dir.2025.253242

Copyright© Author(s) - Available online at dirjournal.org.
Content of this journal is licensed under a Creative Commons Attribution-NonCommercial 4.0 International License.

ABDOMINAL IMAGING

ORIGINAL ARTICLE

The role of T1 hyperintensity in differentiating granulomatous prostatitis from prostate cancer: a retrospective analysis of 31 lesions

Selahattin Durmaz[1]
Mert Kılıç[2,3]
Bilgen Coşkun[4]
Sergin Akpek[4]
Barış Bakır[5]
Tarık Esen[2,3]
Metin Vural[4]
Emre Altınmakas[6,7]

[1]Gaziosmanpaşa Training and Research Hospital, Clinic of Radiology, İstanbul, Türkiye

[2]American Hospital, Clinic of Urology, İstanbul, Türkiye

[3]Koç University School of Medicine, Department of Urology, İstanbul, Türkiye

[4]American Hospital, Clinic of Radiology, İstanbul, Türkiye

[5]İstanbul University İstanbul Faculty of Medicine, Department of Radiology, İstanbul, Türkiye

[6]Icahn School of Medicine at Mount Sinai, Department of Diagnostic, Molecular and Interventional Radiology, New York, USA

[7]Koç University School of Medicine Department of Radiology, İstanbul, Türkiye

Corresponding author: Selahattin Durmaz

E-mail: drselahattindurmaz@gmail.com

Received 06 February 2025; revision requested 19 March 2025; accepted 05 April 2025.

Epub: 20.05.2025

Publication date: xx.xx.2024

DOI: 10.4274/dir.2025.253242

PURPOSE

To investigate the multiparametric magnetic resonance imaging (mpMRI) characteristics of granulomatous prostatitis (GP) and share our experience with 31 pathologically confirmed GP lesions in 19 patients.

METHODS

This two-center retrospective study reviewed the pathological and imaging data of 856 patients who underwent prostate biopsy between January 2012 and April 2024. Of these, 19 patients with available prebiopsy mpMRI and a pathologically confirmed diagnosis of GP were included. Additionally, 280 biopsy-naïve patients diagnosed with clinically significant prostate cancer (csPCa) were included as a control group for comparative analysis. Prebiopsy mpMR images of patients with GP were assessed by consensus between two of three radiologists (M.V., B.C., S.D.), evaluating lesion location, size, shape, multifocality, extraprostatic extension (EPE), signal characteristics on T1-, T2-, and diffusion-weighted imaging (DWI), the mean apparent diffusion coefficient (ADC_{mean}) value, enhancement patterns, and prostate imaging reporting and data system (PI-RADS) scores. Statistical analyses were conducted using SPSS version 30.0.

RESULTS

In 19 patients, 31 pathologically confirmed GP lesions were identified on prebiopsy mpMRI. Twenty-six lesions were located in the peripheral zone and five in the transitional zone. Multifocal involvement was observed in nine patients (47.3%). Thirty of 31 lesions were hypointense on T2-WI, and seven showed capsular bulging and/or irregularity, suggesting EPE. DWI revealed markedly impeded diffusion in all lesions. The median ADC_{mean} value was 825×10^{-3} mm^2/s (IQR: 230×10^{-3} mm^2/s). On dynamic contrast-enhanced sequences, 25 lesions showed early enhancement, five showed prolonged enhancement, and one showed prolonged ring enhancement. Based on mpMRI findings, 17 lesions were assigned a PI-RADS score of 4, and 13 lesions were assigned a PI-RADS score of 5. Notably, 22 lesions (71%) in 14 patients with GP (73.7%) exhibited hyperintensity on T1-WI despite no prior prostate biopsy history. Statistical analysis comparing the GP and csPCa groups revealed that hyperintensity on T1-WI was significantly more frequent in GP, both on a per-patient basis (73.7% vs. 3.2%) and a per-lesion basis (71.0% vs. 3.1%) ($P < 0.0001$ for both).

CONCLUSION

GP shares overlapping imaging features with prostate cancer on mpMRI. However, hyperintensity on T1-WI may serve as a distinguishing feature, potentially reducing unnecessary prostate interventions. Radiologists should consider GP in PI-RADS ≥4 lesions exhibiting T1-WI hyperintensity. Furthermore, given the high incidence of GP following intravesical Bacillus Calmette-Guérin (BCG) therapy, a thorough history of BCG treatment should be obtained.

CLINICAL SIGNIFICANCE

GP is recognized for its tendency to mimic PCa on mpMRI, a finding corroborated by this study. However, T1-WI hyperintensity emerged as a promising distinguishing feature for GP. Incorporating this marker into mpMRI interpretation criteria may help reduce unnecessary prostate interventions and improve patient outcomes.

KEYWORDS

Bacillus Calmette-Guérin, granulomatous prostatitis, magnetic resonance imaging, prostate cancer, T1-weighted imaging

You may cite this article as: Durmaz S, Kılıç M, Coşkun B, et al. The role of T1 hyperintensity in differentiating granulomatous prostatitis from prostate cancer: a retrospective analysis of 31 lesions. *Diagn Interv Radiol.* 20 May 2025 DOI: 10.4274/dir.2025.253242 [Epub Ahead of Print].

Granulomatous prostatitis (GP) is a rare, benign inflammatory condition estimated to account for 3.3% of all inflammatory lesions of the prostate. It has long been recognized that GP lesions can mimic prostate cancer (PCa) in both clinical and laboratory presentations.[1] Typical clinical features include elevated serum prostate-specific antigen (PSA) levels and a firm, nodular prostate on digital rectal examination (DRE).[1,2] On multiparametric magnetic resonance imaging (mpMRI), GP lesions often appear hypointense on T2-weighted images and exhibit markedly impeded diffusion on diffusion-weighted imaging (DWI), closely resembling PCa.[1,3]

The specificity and positive predictive value of mpMRI in detecting PCa have been reported to be limited following intravesical Bacillus Calmette-Guérin (BCG) therapy.[4] In a prospective study, Ogreden et al.[5] compared PSA levels, PSA density (PSAd), DRE findings, and the number of PI-RADS ≥3 lesions detected on mpMRI before and after intravesical BCG therapy in 10 patients. They observed substantially higher PSA and PSAd levels, more frequent abnormal DRE findings, and an increased number of PI-RADS ≥3 lesions after BCG therapy.

The clinical and radiological similarities between GP and PCa often complicate patient management. Most GP lesions receive a high cancer suspicion score (PI-RADS 4 or 5), resulting in unnecessary biopsies.[3,6] Identifying specific mpMRI features of GP may help reduce the number of unnecessary biopsies and their associated complications.

To date, only a limited number of studies—with small patient cohorts—have investigated the MRI characteristics of GP. In this study, we aim to review the existing MRI literature on GP and share our experience with a series of 31 pathologically confirmed GP lesions in 19 patients.

Main points

- Granulomatous prostatitis (GP) shares overlapping imaging characteristics with prostate cancer (PCa) on multiparametric magnetic resonance imaging.
- Hyperintensity on T1-weighted imaging is frequently observed in GP and may assist in distinguishing it from PCa.
- In cases of caseous necrosis or abscess formation, early and prolonged ring enhancement on dynamic contrast-enhanced imaging can support the diagnosis of GP.

Methods

Patients

Koc University Institutional Review Board approved this retrospective observational study and waived the requirement for written informed consent (decision number: 2022.394.IRB1.149, approval date: 10/17/2022). Between January 2012 and April 2024, we reviewed the pathological records of 856 patients who had undergone prostate biopsy due to a high suspicion of clinically significant PCa (csPCa). From this cohort, patients with available prebiopsy mpMRI who were diagnosed with GP through MRI-targeted biopsy—either transrectal MRI-guided in-bore biopsy or MRI-directed cognitive fusion-guided biopsy—were identified and included. Two patients diagnosed with GP via biopsy were excluded due to the absence of detectable lesions on mpMRI.

Additionally, 280 biopsy-naïve patients from the same cohort, diagnosed with csPCa (ISUP grade group ≥2) via biopsy, were included as a control group for comparative analysis. A study flowchart is presented in Figure 1. Clinical data, including age, PSA levels, and PSAd, were also collected for patients with GP.

Magnetic resonance imaging technique

This study included MRI scans from two different hospitals. mpMRI examinations were performed on a 3.0 Tesla scanner (MAGNETOM® Skyra, Siemens AG, Munich, Germany) in 8 patients and a 1.5 Tesla scanner (MAGNETOM® Aera, Siemens AG, Munich, Germany) in 11 patients using a 30-channel phased-array body coil. Prior to imaging, seven patients received an intravenous (IV) injection of 20 mg butylscopolamine (Buscopan®; Boehringer Ingelheim) to suppress bowel peristalsis.

All patients underwent mpMRI due to elevated serum PSA levels and/or suspicious findings on DRE. The imaging protocol included axial T1-WI of the pelvis, high-resolution T2-WI in axial, coronal, and sagittal planes, axial DWI, and axial dynamic contrast-enhanced (DCE) sequences, performed according to the recommendations of the European consensus meeting on prostate mpMRI standardization.[7] DCE images were obtained using 9–10 mL of gadolinium-based contrast agent (gadoterate meglumine 0.5 mmol/mL; DOTAREM®, Guerbet, Villepinte, France), administered at a rate of 3.5 mL/s via power injector. MRI protocols for both centers are summarized in Table 1.

Image analysis

All MRI were reviewed in consensus by two of three radiologists (M.V., B.C., S.D.) with 4–16 years of experience in prostate MRI. The reviewers were blinded to the pathological results. Each GP lesion was evaluated for location, shape, size, multifocality, signal intensity (SI) on T1-WI, T2-WI, and DWI, mean apparent diffusion coefficient (ADC_{mean}) value, presence of extraprostatic extension (EPE), enhancement patterns on DCE, and PI-RADS score. The PI-RADS scores were assigned according to the criteria outlined in PI-RADS version 2.1.[8] Lesion shape was assessed on T2-WI using the shape patterns described by Suzuki et al.[9]

SI on T1-WI, T2-WI, and DWI was assessed by visual comparison with the residual healthy peripheral zone (PZ). Mean ADC values were measured by placing a region of interest over the largest area of the lesion, avoiding the tumor edges. For comparative analysis, the T1-WI signal characteristics of csPCa lesions in the control group were also retrospectively assessed and recorded.

Statistical analysis

Statistical analyses were performed using SPSS version 30.0 (IBM Corp., Armonk, NY, USA). Continuous variables were assessed for normality using the Shapiro-Wilk test. Non-normally distributed variables were summarized as median with interquartile range (IQR), whereas normally distributed variables were reported as mean ± standard deviation. Categorical variables were presented as frequencies and percentages. The presence of hyperintensity on T1-WI was compared between the csPCa and GP groups using Fisher's exact test on both a per-patient and per-lesion basis. A P value of < 0.05 was considered statistically significant.

Results

A total of 31 pathologically proven GP lesions in 19 patients were included in this study. The overall incidence of GP in our cohort was 21/856 (2.4%). Eleven patients had a history of intravesical BCG therapy and were considered to have BCG-induced GP, whereas the remaining patients had no identifiable predisposing factors and were thus classified as having idiopathic (non-specific) GP. In all patients, the interval between the last BCG administration and the mpMRI examination was less than 3 months.

The median age was 65 years IQR: 13.5 years), the median PSA level was 6.25 ng/

mL (IQR: 2.8 ng/mL), the median PSAd was 0.14 ng/mL/mL (IQR: 0.08 ng/mL/mL), and the median prostate volume was 47 mL (IQR: 22 mL). mpMRI evaluation identified 26 lesions in the PZ and five in the transition zone. Both zones were involved in three patients (Figure 2). Lesions were classified by shape as nodular (n = 25), diffuse (n = 5), or cystic (n = 1). The median lesion size was 14 mm (IQR: 11.25 mm). Multifocal involvement was present in nine patients (Figures 2 and 3).

Regardless of lesion shape, 22 lesions (71%) in 14 patients with GP (73.7%) demonstrated increased SI on T1-WI (Figures 2 and 4). In the control group, only nine lesions (3.1%) in nine patients (3.2%) exhibited mild to moderate T1 hyperintensity. Statistical analysis showed that hyperintensity on T1-WI was significantly more frequent in GP compared with csPCa, both on a per-patient basis [14/19 (73.7%) vs. 9/280 (3.2%), $P < 0.0001$] and on a per-lesion basis [22/31 (71.0%) vs. 9/294 (3.1%), $P < 0.0001$].

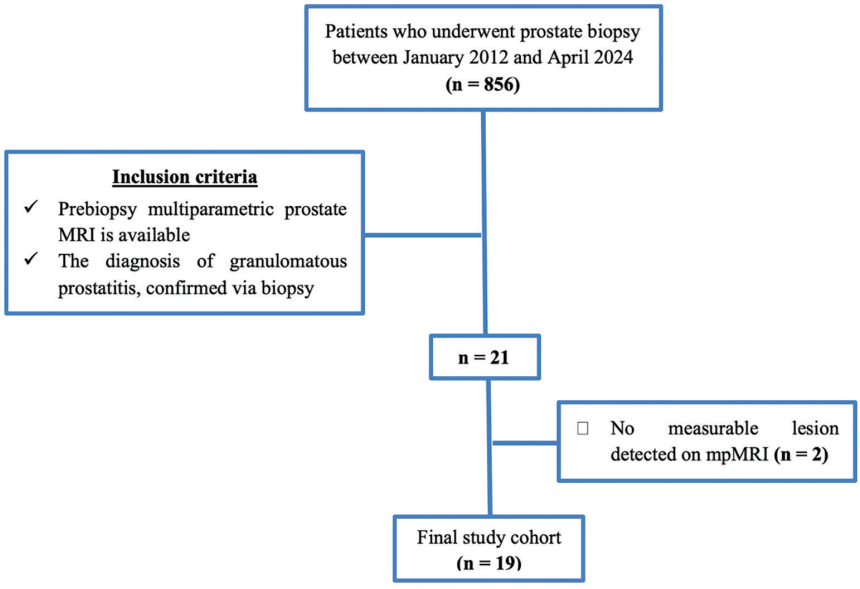

Figure 1. The study flowchart. MRI, magnetic resonance imaging; mpMRI, multiparametric magnetic resonance imaging.

On DWI, all lesions demonstrated markedly impeded diffusion. The median ADC_{mean} value was 825×10^{-3} mm^2/s (IQR: 230×10^{-3} mm^2/s). On T2-WI, 30 lesions were hypointense, whereas the remaining lesion was iso- to hyperintense compared with the PZ. Capsular bulging and/or irregularity suggestive of EPE was noted in seven lesions (Figures 3 and 4). Following IV contrast administration, 25 lesions showed early enhancement (Figures 2 and 4), five showed prolonged enhancement, and one demonstrated prolonged ring enhancement (Figure 5). The characteristics of the patients and the main mpMRI findings of the lesions are presented in Table 2.

Based on imaging findings, 13 lesions were assigned a PI-RADS 5 score, and 17 lesions were scored as PI-RADS 4. The remaining lesion's MRI features were consistent with abscess formation. Due to the high clinical suspicion of PCa, seven patients underwent MRI-guided in-bore biopsy, and 11 underwent MRI-directed cognitive fusion-guided biopsy. The remaining patient—suspected to have a prostate abscess—was also sampled by MRI-directed cognitive fusion-guided biopsy to confirm the diagnosis and rule out coexisting PCa.

Histopathological examination confirmed the diagnosis of GP in all patients. Concomitant PCa was detected outside the targeted lesion in four patients: three with a Gleason score of 6 (3+3) (cases 7, 13, and 17) and one with a Gleason score of 8 (4+4) (case 14).

Table 1. Multiparametric magnetic resonance imaging protocols of two centers

Parameter	Center	T2-WI	DWI	DCE	T1-WI
TR (ms)	1	5290	4800	9	445
	2	7500	4700	4.27	578
TE (ms)	1	111	98	1.76	9.80
	2	101	59	1.64	10
Field of view (mm)	1	200 × 200	260 × 260	260 × 260	300 × 400
	2	200 × 200	192 × 192	200 × 200	200 × 200
Matrix size	1	512 × 297	192 × 154	192 × 155	384 × 297
	2	320 × 230	128 × 128	192 × 134	192 × 256
Slice thickness/gap (mm)	1	3/0.6	3.6/0	3.6/0	6/1.2
	2	3	3	3	3
Flip angle (°)	1	180	180	15	120
	2	160		12	160
Scan time (mins)	1	03:23	05:38	04:38	1:16
	2	04:17	08:34	04:53	2:31
Temporal resolution (s)	1	-	-	8	-
	2	-	-	8	-
B value	1	-	1600	-	-
	2	-	1400	-	-

TR, repetition time; TE, echo time; T2-WI, T2-weighted imaging; DWI, diffusion-weighted imaging; T1-WI, T1-weighted imaging; DCE, Dynamic contrast-enhanced.

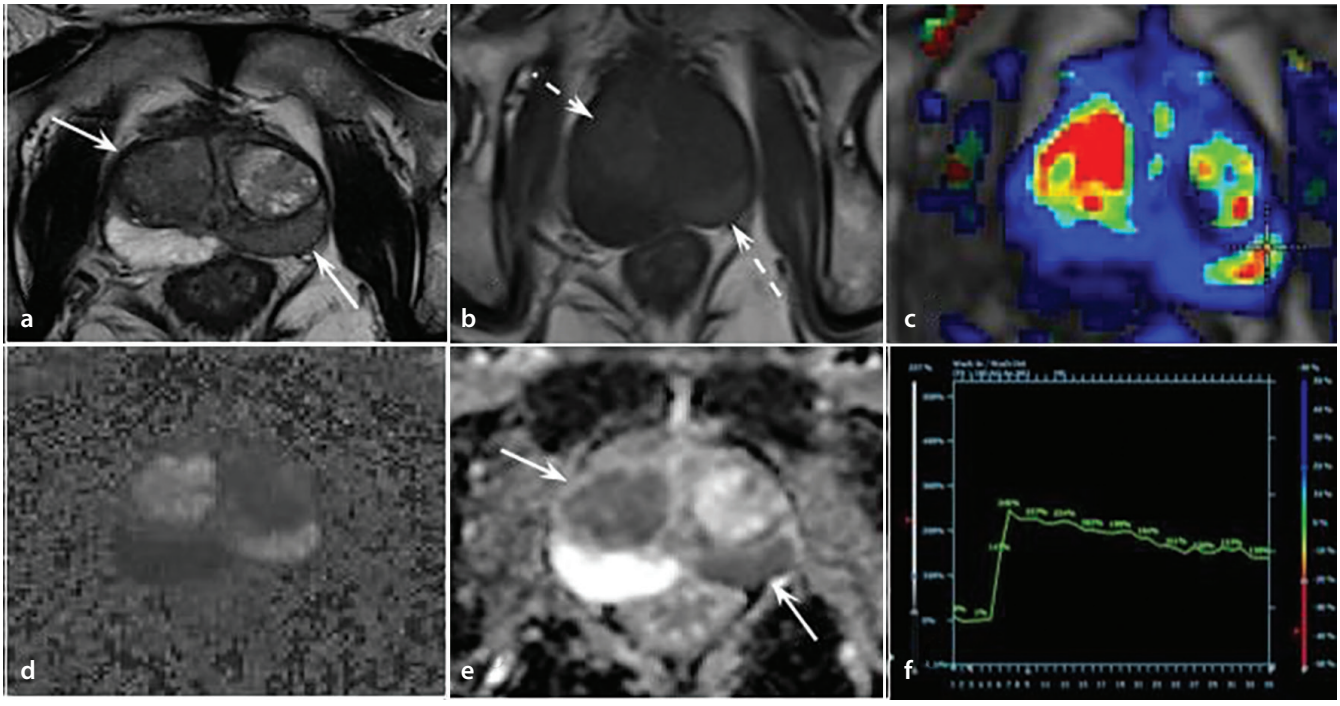

Figure 2. A 76-year-old biopsy-naïve patient (case 4) with a history of intravesical BCG administration for non–muscle-invasive bladder cancer presented with elevated PSA (9.79 ng/mL) and abnormal digital rectal examination. The prostate volume and PSA density were 76 mL and 0.13 ng/mL^2, respectively. Subsequent mpMRI demonstrated 21 mm left peripheral zone and 29 mm right transition zone lesions. Both lesions showed a hypointense signal on T2-WI (arrows) **(a)** and a hyperintense signal on T1-WI (dashed arrows) **(b)**, with marked restricted diffusion on DWI and ADC maps (ADC values: 825 and 758 × 10^{-3} mm^2/s) **(d, e)**. On DCE imaging **(c, f)**, both lesions showed early enhancement relative to the background prostate gland and were classified as PI-RADS 5. BCG, Bacillus Calmette-Guérin; PSA, prostate-specific antigen; mpMRI, multiparametric magnetic resonance imaging; T1-WI, T1-weighted imaging; T2-WI, T2-weighted imaging; DWI, Diffusion-weighted imaging; ADC, apparent diffusion coefficient; PI-RADS, prostate imaging reporting and data system; DCE, dynamic contrast-enhanced.

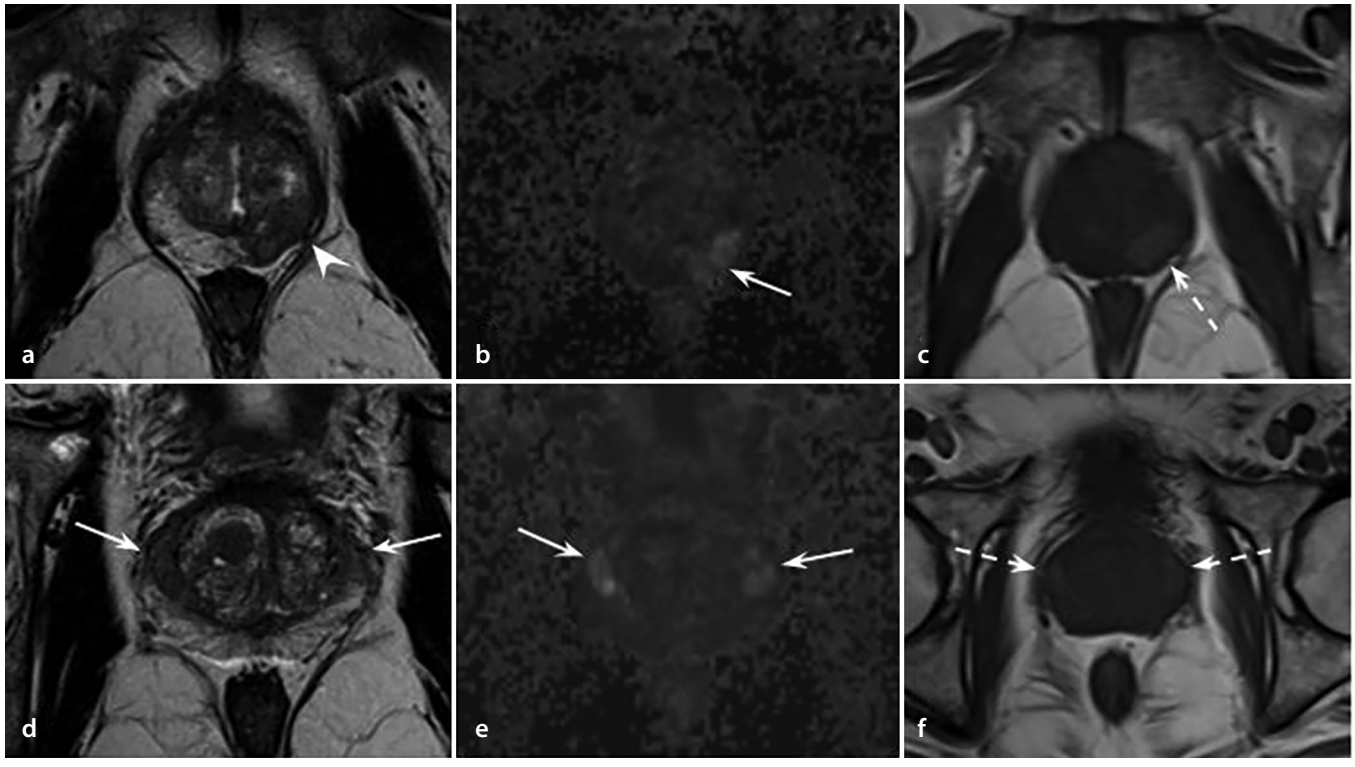

Figure 3. A 76-year-old biopsy-naïve patient (case 7) with a history of intravesical BCG administration for non–muscle-invasive bladder cancer presented with elevated PSA (5.2 ng/mL) and abnormal digital rectal examination findings. The prostate volume and PSA density were 37 mL and 0.14 ng/mL^2, respectively. Subsequent mpMRI demonstrated three peripheral zone lesions measuring 11 mm, 12 mm, and 19 mm. The lesions showed a hypointense signal on T2-WI **(a, d)** and a hyperintense signal on T1-WI **(c, f)** (dashed arrows), with marked impeded diffusion (ADC values: 737, 925, and 675 × 10^{-3} mm^2/s) **(b, e)**. Note capsular bulging and mild irregularity on T2-WI **(a)** (arrowhead), suggesting EPE. BCG, Bacillus Calmette-Guérin; PSA, prostate-specific antigen; T2-WI, T2-weighted imaging; T1-WI, T1-weighted imaging; ADC, apparent diffusion coefficient; EPE, extraprostatic extension.

Table 2. The summary of the clinical, demographic, and multiparametric magnetic resonance imaging features of the patients

Case	Age (years)	PSA (ng/mL)	PSAd (ng/mL^2)	BCG history	Number of lesions	Location	Shape	SI on T2-WI	SI on DWI	SI on T1-WI	Enhancement pattern	PI-RADS score
1	62	9	0.1	+	1	PZ	Cystic	Iso-high	High	Iso	Prolonged-ring	-
2	54	3.6	0.06	+	1	PZ	Diffuse	Low	High	High	Prolonged	5
3	72	6	0.23	+	2	PZ	Nodular	Low	High	High	Early	4
4	76	9.79	0.13	+	2	PZ TZ	Nodular	Low	High	High	Early	5
5	74	4.4	0.1	+	1	PZ	Nodular	Low	High	High	Early	4
6	73	4.11	0.1	+	1	PZ	Nodular	Low	High	High	Early	5
7	76	5.2	0.14	+	3	PZ	Nodular	Low	High	High	Early	4 4 5
8	74	5	0.19	+	2	PZ	Nodular	Low	High	High	Early Prolonged	4
9	63	7	0.032	-	1	PZ	Diffuse	Low	High	High	Early	5
10	51	4	0.2	-	2	PZ	Nodular	Low	High	Iso	Early	4
11	70	6.52	0.1	-	1	PZ	Nodular	Low	High	High	Early	5
12	57	9.9	0.24	-	3	PZ TZ TZ	Nodular Diffuse Diffuse	Low	High	High	Early	5 4 (3 + 1) 4 (3 + 1)
13	68	5.54	0.13	-	1	PZ	Diffuse	Low	High	Iso	Early	5
14	65	10	0.16	-	1	PZ	Nodular	Low	High	High	Early	5
15	53	6.5	0.14	-	2	TZ	Nodular	Low	High	Iso	Early	5
16	65	11.23	0.24	+	1	PZ	Nodular	Low	High	High	Prolonged	4
17	61	5.23	0.1	-	1	PZ and TZ	Nodular	Low	High	Iso	Early	5
18	56	6.5	0.16	+	3	PZ	Nodular	Low	High	High High Iso	Early	4
19	62	8.1	0.16	+	2	PZ	Nodular	Low	High	High Iso	Prolonged	4

PSA, prostate-specific antigen; PSAd, prostate-specific antigen density; BCG, Bacillus Calmette-Guérin; PZ, peripheral zone; TZ, transition zone; SI, signal intensity; T2-WI, T2-weighted imaging; DWI, diffusion-weighted imaging; T1-WI, T1-weighted imaging; PI-RADS, prostate imaging reporting and data system.

Table 3. Reported case series of granulomatous prostatitis in the English literature

First author (reference)	Year	Patient (n)	BCG history (n%)	Age (years)	PSA (ng/ml)	PSAd (ng/mL^2)	Lesion size (mm)	Location PZ (n)/TZ (n)	Low SI on T2WI (n%)	High SI on DWI (n%)	High SI on T1-WI (n%)
Naik et al.[16]	1998	10	0	68	11	-	-	-	40	-	0
Ma et al.[17]	2009	5	100	-	-	-	-	5/0	100	-	-
Bour et al.[15]	2012	5	60	-	-	-	-	5/4	80	100	0
Suzuki et al.[9]	2013	10	100	70.2	7.39	-	-	10/2	90	90	70
Kawada et al.[22]	2015	5	100	70.4	-	-	21.2	5/3	40	100	100
Gottlieb et al.[2]	2017	6	100	68.7	-	-	-	6/0	100	17	0
Rais-Bahrami et al.[19]	2017	5	40	66	7.4	0.20	19.2	3/2	100	100	-
Lee et al.[1]	2019	16	0	62.5	7.7	0.15	-	16/14	100	100	-
Wang et al.[24]	2021	8	100	63.6	5.7	-	-	8/0	100	100	12.5
Lee et al.[23]	2022	24	100	66	-	-	22	-	100	92	-
Bertelli et al.[14]	2022	11	36	68	8.74	0.12	-	10/4	100	100	-
Ogreden et al.[5]	2024	10	100	66.9	4.3	0.10	-	-	-	-	-
Guerra et al.[26]	2024	12	100	62	7.26	0.13	10	9/7	83	100	-
Avudaiappan et al.[4]	2024	7	100	-	6.9	-	-	5/0	-	-	-

BCG, Bacillus Calmette-Guérin; PSA, prostate-specific antigen; PSAd, prostate-specific antigen density; PZ, peripheral zone; TZ, transition zone; SI, signal intensity; T2-WI, T2-weighted imaging; DWI, Diffusion-weighted imaging; T1-WI, T1-weighted imaging.

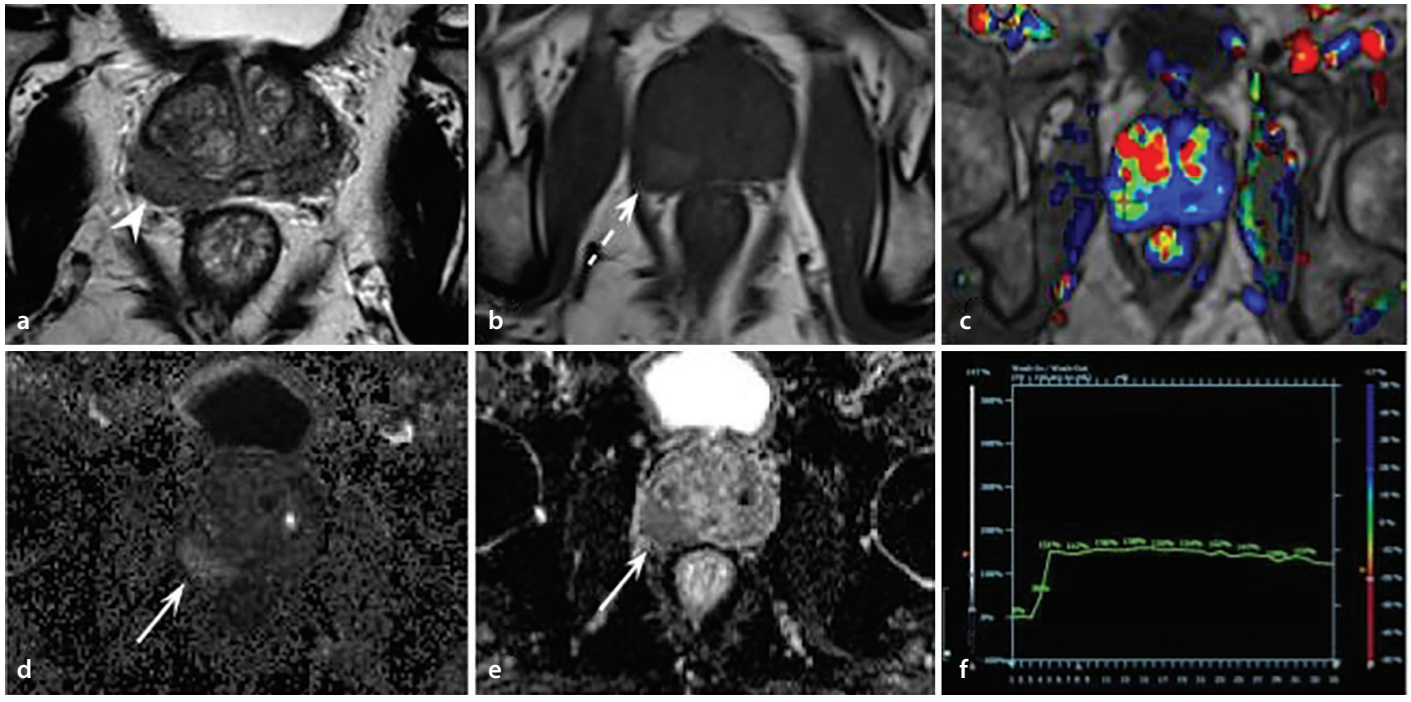

Figure 4. A 73-year-old biopsy-naïve patient (case 6) with a history of intravesical BCG administration for non–muscle-invasive bladder cancer presented with elevated PSA (4.11 ng/mL) and abnormal digital rectal examination findings. The prostate volume and PSA density were 47 mL and 0.10 ng/mL^2, respectively. Subsequent mpMRI revealed a 25 mm right peripheral zone lesion. The lesion demonstrated a hypointense signal on T2-WI **(a)** and a hyperintense signal on T1-WI **(b)** (dashed arrow), with marked impeded diffusion (ADC value: 814 × 10^{-3} mm^2/s) **(d, e)**. On DCE imaging **(c, f)**, the enhancement pattern resembled that of prostate cancer. Note the capsular bulging and irregularity on T2-WI **(a)** (arrowhead), suggestive of EPE. BCG, Bacillus Calmette-Guérin; PSA, prostate-specific antigen; mpMRI, multiparametric magnetic resonance imaging; T2-WI, T2-weighted imaging; T1-WI, T1-weighted imaging; ADC, apparent diffusion coefficient; DCE, dynamic contrast-enhanced.

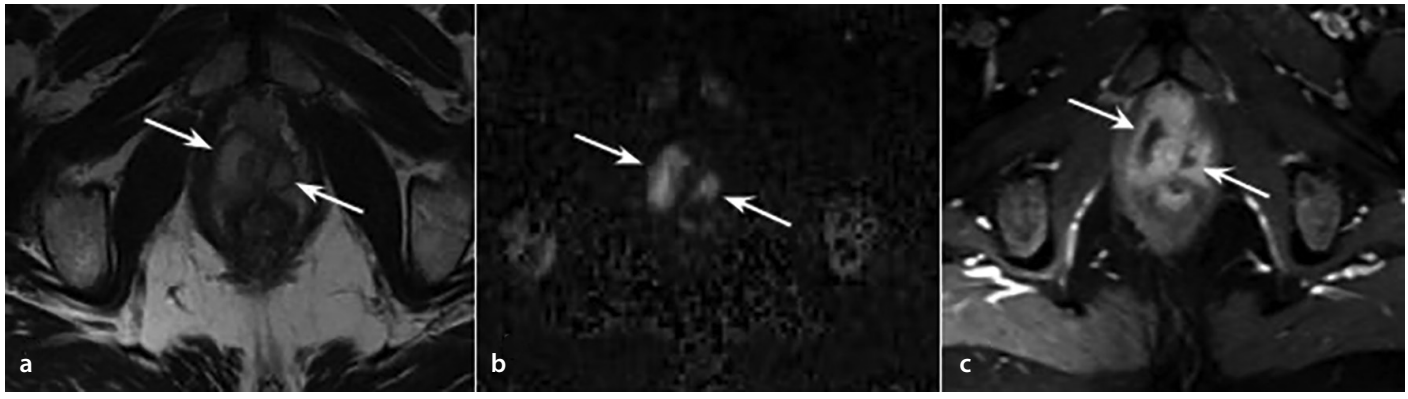

Figure 5. A 62-year-old biopsy-naïve patient (case 1) with a history of intravesical BCG administration for non–muscle-invasive bladder cancer presented with elevated PSA (9 ng/mL) and abnormal digital rectal examination. The prostate volume and PSA density were 86 mL and 0.10 ng/mL^2, respectively. Subsequent mpMRI demonstrated a peripheral zone lesion located at the apex (arrows). The lesion appeared iso- to hyperintense on T2-WI **(a)** and isointense on T1-WI (not shown). On DCE imaging **(c)**, peripheral rim-like enhancement was observed (arrowhead). The avascular central portion of the lesion demonstrated marked impeded diffusion (ADC value: 715 × 10^{-3} mm^2/s) **(b)**. BCG, Bacillus Calmette-Guérin; PSA, prostate-specific antigen; mpMRI, multiparametric magnetic resonance imaging; T2-WI, T2-weighted imaging; T1-WI, T1-weighted imaging; ADC, apparent diffusion coefficient; DCE, dynamic contrast-enhanced.

Discussion

In this study, we found that GP and PCa have overlapping imaging features on mpMRI; however, we also identified hyperintensity on T1-WI as a promising distinguishing feature for GP.

GP can be idiopathic (non-specific) or secondary to infective (intravesical BCG therapy) etiologies, iatrogenic factors [transurethral resection of the prostate (TUR-P), prostate biopsy], or systemic diseases.[1,10] According to reported series, non-specific GP comprises 60%–77.7% of all GP cases.[10] However, in our patient group, the proportions of non-specific and BCG-induced GP cases were 42% (8/19) and 58% (11/19), respectively. This discrepancy, compared with a more extensive series, can be attributed to our small sample size and the high proportion of patients with a history of intravesical BCG therapy for the treatment of bladder cancer. The incidence of GP following intravesical BCG therapy is reported to be 41%.[1]

Oppenheimer et al.[11] reported the incidence of GP to be 0.36% in a series of 25,000

men who underwent prostate biopsy. However, based on more recent studies, the incidence has been increasing due to the widespread use of intravesical BCG therapy, the growing number of TUR-P procedures, and the increasing frequency of extensive prostate biopsies.[3,12,13] Similar to these more recent studies,[1,13,14] the GP incidence in our cohort was 2.4%.

GP lesions are usually asymptomatic, except for infectious GP, which generally does not require treatment.[14,15] However, the primary concern lies in the potential for these lesions to be misinterpreted as PCa on mpMRI, leading to unnecessary biopsy. A limited number of studies have explored the MRI characteristics of GP to address this radiology-pathology discordance and improve the positive predictive value of MRI. Table 3 summarizes the reported GP case series in the English literature.

Naik and Carey[16] were among the first to investigate the imaging characteristics of GP in an attempt to identify specific features. They evaluated the transrectal ultrasound and MRI (T2-WI, pre- and post-contrast T1-WI) findings of 10 patients diagnosed with GP. They concluded that no reliable clinical, laboratory, US, or MRI findings could be used to differentiate GP from PCa. Ma et al.[17] evaluated MRI findings in five patients with GP and observed diffuse or focal-nodular decreased SI on T2-WI. Since neither the clinical nor imaging findings could reliably exclude the possibility of PCa, the researchers stated that a biopsy was necessary for a definitive diagnosis.[17]

Five biopsy-proven patients with GP (three of whom had a history of BCG therapy) were reported by Bour et al.[15] Based on mpMRI findings, two distinct manifestations of GP were described. The first and more frequent type had a tumor-like appearance that could not be distinguished from that of PCa. In contrast, the second type was suggestive of abscess formation induced by a severe caseating necrotic process. Furthermore, the authors observed periprostatic or seminal vesicle wall infiltration in four patients, simulating locally advanced PCa.[15]

Lee et al.[1] evaluated the MRI findings of 16 patients with GP and reported suspicious EPE findings in 15 of them. All patients were assigned a PI-RADS score of five according to PI-RADS version 2.[18] In another study, Rais-Bahrami et al.[19] compared the clinical and mpMRI findings of five biopsy-proven patients with GP (two with a history of BCG therapy) to 15 biopsy-proven csPCa patients. In contrast to the findings of Lee et al.[1] and Bour et al.,[15] they reported significantly higher ADC values in patients with GP compared to those with PCa and suggested that high-stage features such as EPE are more indicative of PCa than GP. Another study comparing BCG-exposed and non-BCG-exposed groups reported a lower risk of csPCa in PI-RADS ≥3 lesions among BCG-exposed patients.[20]

Our findings were consistent with those of Lee et al.[1] and Bour et al.[15]. In our cohort, 30 lesions exhibited a tumor-like appearance with low ADC_{mean} values, seven of which showed capsular bulging and/or irregularity suggestive of EPE (Figures 3 and 4). The remaining lesion displayed imaging findings consistent with the second manifestation described by Bour et al.[15]

GP tends to show variable diffusion characteristics. Since the degree of impeded diffusion reflects cellular density, it is thought that more acute manifestations of GP tend to exhibit greater diffusion restriction.[2,3,21] Gottlieb et al.[2] evaluated the mpMRI findings of six patients with BCG-induced GP. Based on the diffusion characteristics of the lesions, the authors described acute and chronic patterns, which were believed to reflect the acute and chronic phases of prostatitis, respectively. The chronic pattern was more common and demonstrated less impeded diffusion, whereas the acute pattern was indistinguishable from aggressive PCa.[2] A case report by Logan et al.[12] evaluated the serial MRI changes in BCG-induced GP from the completion of BCG therapy to the development of GP. The authors noted that the manifestation of chronic GP took more than 12 months following the completion of BCG therapy.[12] In our cohort, the interval between the last BCG administration and mpMRI examination was less than 3 months in all patients. Accordingly, we observed marked impeded diffusion in all cases, corresponding to the acute manifestation of GP.

The dynamic contrast enhancement pattern of BCG-induced GP lesions was first evaluated by Kawada et al.[22] in five patients. They reported that early and prolonged ring enhancement may help differentiate GP from PCa. Additionally, the authors noted T1-WI hyperintensity in all patients. Another study involving four BCG-induced GP and seven non-specific GP patients also observed prolonged ring enhancement in the BCG-induced cases.[14] In our study group, prolonged ring enhancement was observed in one patient (case 1) with a history of intravesical BCG therapy (Figure 5). Among the remaining patients, 25 out of 30 lesions (83%) demonstrated early enhancement similar to PCa, whereas five lesions showed prolonged enhancement.

The largest group of BCG-induced GP patients (n = 24) was reported by Lee et al.[23] Based on imaging findings from contrast-enhanced T1-WI and DWI, the authors categorized GP lesions into three types: type A, type B, and type C. Types A and B were reported to correspond to the acute phase of BCG-induced GP, whereas type C represented the chronic phase. As previously stated by Gottlieb et al.,[2] the acute manifestation—particularly type A lesions—was reported to be more challenging to differentiate from PCa. According to the imaging patterns proposed by Lee et al.,[23] 30 lesions in our cohort could be classified as type A, and the remaining lesion as type B.

Suzuki et al.[9] performed a bi-parametric MRI on ten patients with BCG-induced GP and identified three main lesion patterns based on shape: diffuse, nodular, and cystic with a mural nodule. In all diffuse lesions, the authors observed hyperintensity on T1-WI.[9] In another study, 12.5% (n = 2/8) of BCG-induced GP cases were reported to show hyperintensity on T1-WI.[24] Supporting this, Lim et al.[25] also noted hyperintensity on T1-WI in a case of mass-forming splenic tuberculosis.

In our patient group, 31 pathologically confirmed GP lesions were identified. Similar to a recently published study,[26] the majority of GP lesions in our cohort (n = 25/31, 80.6%) were nodular in shape. Regardless of lesion shape, 22 lesions (71%) demonstrated hyperintensity on T1-WI. All patients in our cohort were biopsy-naïve, and histopathological examination did not reveal any findings that could account for this hyperintensity. Previous studies have attributed the hyperintense appearance of granulomatous lesions on T1-WI to the presence of paramagnetic substances, such as macrophage-laden oxygen free radicals produced during phagocytosis by activated macrophages.[6,9,27,28]

To the best of our knowledge, this study reports the mpMRI characteristics of the largest number of GP lesions. On a per-patient basis, our study includes one of the largest groups of patients with GP. Based on the mpMRI findings in our patient group, we suggest that hyperintensity on T1-WI can be helpful in the differentiation of GP from PCa. As discussed above, hyperintensity on T1-WI has been observed in three previous studies as an MRI finding in some GP lesions.[9,22,24] However, to our knowledge, this is the first

time it is being reported and highlighted as a possible differentiator of GP from PCa.

We acknowledge that this study had several limitations. First, our cohort is relatively small; however, this can be attributed to the low incidence of GP. Furthermore, as far as we can tell, it is one of the most extensive series among published studies on the MRI findings of GP. Second, there may be increased patient selection bias owing to the retrospective design and the recruitment period spanning 12 years.

In conclusion, despite advances in MRI technology and imaging techniques, differentiating GP from PCa based on mpMRI findings remains challenging. However, we propose hyperintensity on T1-WI as a promising feature in this differentiation. To avoid unnecessary prostate interventions, radiologists should consider the possibility of GP in PI-RADS ≥4 lesions that exhibit hyperintensity on T1-WI. Additionally, given the high incidence of GP following intravesical BCG therapy, a detailed history of BCG treatment should be carefully investigated. Prospective studies with larger patient cohorts are needed to validate the diagnostic value of our findings.

Footnotes

Conflict of interest disclosure

The authors declared no conflicts of interest.

References

1. Lee SM, Wolfe K, Acher P, Liyanage SH. Multiparametric MRI appearances of primary granulomatous prostatitis. *Br J Radiol*. 2019;92(1098):20180075. [Crossref]
2. Gottlieb J, Princenthal R, Cohen MI. Multiparametric MRI findings of granulomatous prostatitis developing after intravesical bacillus calmette-guérin therapy. *Abdom Radiol (NY)*. 2017;42(7):1963-1967. [Crossref]
3. Gaudiano C, Renzetti B, De Fino C, et al. Multiparametric magnetic resonance imaging for the differential diagnosis between granulomatous prostatitis and prostate cancer: a literature review to an intriguing diagnostic challenge. *Front Oncol*. 2023;13:1178430. [Crossref]
4. Avudaiappan AP, Prabhakar P, Siretskiy R, Renshaw A, Eldefrawy A, Manoharan M. Reliability of mpMRI in diagnosing cancer prostate following intravesical BCG for bladder cancer. *BJUI Compass*. 2024;5(11):1090-1094. [Crossref]
5. Ogreden E, Oguz U, Demirelli E, et al. The role of multiparametric magnetic resonance ımaging in the diagnosis of granulomatous prostatitis mimicking prostate cancer. *Abdom Radiol (NY)*. 2024;49(7):2305-2310. [Crossref]
6. Han C, Zhu L, Liu X, Ma S, Liu Y, Wang X. Differential diagnosis of uncommon prostate diseases: combining mpMRI and clinical information. *Insights Imaging*. 2021;12(1):79. [Crossref]
7. Dickinson L, Ahmed HU, Allen C, et al. Magnetic resonance imaging for the detection, localisation, and characterisation of prostate cancer: recommendations from a European consensus meeting. *Eur Urol*. 2011;59(4):477-494. [Crossref]
8. Turkbey B, Rosenkrantz AB, Haider MA, et al. Prostate imaging reporting and data system version 2.1: 2019 update of prostate imaging reporting and data system version 2. *Eur Urol*. 2019;76(3):340-351. [Crossref]
9. Suzuki T, Takeuchi M, Naiki T, et al. MRI findings of granulomatous prostatitis developing after intravesical Bacillus Calmette-Guérin therapy. *Clin Radiol*. 2013;68(6):595-599. [Crossref]
10. Kitzing YX, Prando A, Varol C, Karczmar GS, Maclean F, Oto A. Benign conditions that mimic prostate carcinoma: MR imaging features with histopathologic correlation. *Radiographics*. 2016;36(1):162-175. [Crossref]
11. Oppenheimer JR, Kahane H, Epstein JI. Granulomatous prostatitis on needle biopsy. *Arch Pathol Lab Med*. 1997;121(7):724-729. [Crossref]
12. Logan JK, Walton-Diaz A, Rais-Bahrami S, et al. Changes observed in multiparametric prostate magnetic resonance imaging characteristics correlate with histopathological development of chronic granulomatous prostatitis after intravesical Bacillus Calmette-Guerin therapy. *J Comput Assist Tomogr*. 2014;38(2):274-276. [Crossref]
13. Shukla P, Gulwani HV, Kaur S. Granulomatous prostatitis: clinical and histomorphologic survey of the disease in a tertiary care hospital. *Prostate Int*. 2017;5(1):29-34. [Crossref]
14. Bertelli E, Zantonelli G, Cinelli A, et al. Granulomatous prostatitis, the great mimicker of prostate cancer: can multiparametric MRI features help in this challenging differential diagnosis? *Diagnostics (Basel)*. 2022;12(10):2302. [Crossref]
15. Bour L, Schull A, Delongchamps NB, et al. Multiparametric MRI features of granulomatous prostatitis and tubercular prostate abscess. *Diagn Interv Imaging*. 2013;94(1):84-90. [Crossref]
16. Naik KS, Carey BM. The transrectal ultrasound and MRI appearances of granulomatous prostatitis and its differentiation from carcinoma. *Clin Radiol*. 1999;54(3):173-175. [Crossref]
17. Ma W, Kang SK, Hricak H, Gerst SR, Zhang J. Imaging appearance of granulomatous disease after intravesical Bacille Calmette-Guerin (BCG) treatment of bladder carcinoma. *AJR Am J Roentgenol*. 2009;192(6):1494-1500. [Crossref]
18. Weinreb JC, Barentsz JO, Choyke PL, et al. PI-RADS Prostate imaging - reporting and data system: 2015, version 2. *Eur Urol*. 2016;69(1):16-40. [Crossref]
19. Rais-Bahrami S, Nix JW, Turkbey B, et al. Clinical and multiparametric MRI signatures of granulomatous prostatitis. *Abdom Radiol (NY)*. 2017;42(7):1956-1962. [Crossref]
20. Rodríguez Cabello MA, Méndez Rubio S, Vázquez Alba D, Aulló González C, Platas Sancho A. Effect of Bacillus Calmette-Guerin exposure on prostate cancer detection using magnetic resonance imaging: a cohort study. *Clin Genitourin Cancer*. 2024;22(5):102130. [Crossref]
21. Green DB, Kawashima A, Menias CO, et al. Complications of Intravesical BCG immunotherapy for bladder cancer. *Radiographics*. 2019;39(1):80-94. [Crossref]
22. Kawada H, Kanematsu M, Goshima S, et al. Multiphase contrast-enhanced magnetic resonance imaging features of Bacillus Calmette-Guerin-induced granulomatous prostatitis in five patients. *Korean J Radiol*. 2015;16(2):342-348. [Crossref]
23. Lee S, Oh YT, Kim HM, Jung DC, Hong H. Imaging patterns of Bacillus Calmette-Guérin-related granulomatous prostatitis based on multiparametric MRI. *Korean J Radiol*. 2022;23(1):60-67. [Crossref]
24. Wang Z, Han C, Xu Y, et al. The role of prostate-specific antigen and multiparametric magnetic resonance imaging in the diagnosis of granulomatous prostatitis induced by intravesical Bacillus Calmette-Guérin vaccine therapy in patients with nonmuscle invasive bladder cancer. *J Cancer Res Ther*. 2021;17(3):625-629. [Crossref]
25. Lim J, Yu JS, Hong SW, Chung JJ, Kim JH, Kim KW. A case of mass-forming splenic tuberculosis: MRI findings with emphasis of diffusion-weighted imaging characteristics. *J Korean Med Sci*. 2011;26(3):457-460. [Crossref]
26. Guerra J, Pina JM, Andrade V, Lança M, Campos Pinheiro L. Bacillus Calmette-Guérin instillations may mimic prostate cancer on multiparametric magnetic resonance imaging. *Cureus*. 2024;16(9):e69890. [Crossref]
27. Chung MH, Lee HG, Kwon SS, Park SH. MR imaging of solitary pulmonary lesion: emphasis on tuberculomas and comparison with tumors. *J Magn Reson Imaging*. 2000;11(6):629-637. [Crossref]
28. Sze G, Zimmerman RD. The magnetic resonance imaging of infections and inflammatory diseases. *Radiol Clin North Am*. 1988;26(4):839-859. [Crossref]